formation of numerous small domains, which accumulate and fuse into recurrent patterns, suggesting a curvature preference of coexisting domains (Fig. 2g and h). In both cases, the L_d phase is observed to favour saddle shapes, and the high-curvature tip region of the arms of the starfish vesicle (Fig. 2h), which again indicates smaller magnitudes of bending rigidities of L_d phases compared to L_o phase domains, which preferentially segregate into the lower-curvature tubular areas (Fig. 2g and h). Owing to the high temperature and the particular membrane composition, line tension effects are expected to be small in both cases. Note that domains in the essentially flat central body of the starfish vesicle are randomly distributed, as they do not experience a significant curvature gradient.

The experimental approach and observations described here allow us to address two-dimensional critical phenomena, the influence of membrane additives on line tension, and to test and advance theories on membrane shape. Some of our observations may furthermore have analogues in fundamental biological membrane processes[26,27]. □

Methods

Vesicle preparation

GUVs were mostly prepared by the method of electroswelling[28], at a temperature of 60 °C, in a solution of 100 mM sucrose. Using GUVs prepared in 50 mM KCl led to virtually the same phenomena observed at zero ionic strength. Lipid mixtures composed of varying fractions of sphingomyelin (from egg), dioleoylphosphatidylcholine and cholesterol were used. The elevated temperature ensured that GUVs were formed from swollen lipid membranes above the upper critical mixing/demixing temperature of L_o/L_d phase coexistence. The mixing/demixing temperature, T_m, varied with composition (see Supplementary Information for further details). Phase coexistence was observed at temperatures up to 56 ± 0.2 °C.

Fluorescence labelling

GUVs were labelled with two differentially partitioning membrane probes in order to distinguish between L_o and L_d domains. The headgroup labelled lipid probe N-lissamine rhodamine dipalmitoylphosphatidylethanolamine (rho-DPPE) partitioned so effectively into L_d domains that in many cases (depending on the membrane composition) no fluorescence in the coexisting L_o phase domains could be detected. The same behaviour was found for numerous other fluorescence-labelled lipid or fatty acid analogues, including the widely used amphiphilic indocarbocyanine dye DiI. We found that the polycyclic aromatic hydrocarbon dye perylene (among other polycyclic aromatic dyes of similar type) partitions preferentially into the L_o phase. The partitioning is, however, weaker compared to rho-DPPE. Rho-DPPE was added at 1/1,000 (dye/lipid). Perylene was added at 1/500. The only charged component in the lipid mixture used in the present study is the fluorescence probe rho-DPPE. In independent experiments using an uncharged lipid label, we confirmed the occurrence of modulated phases.

Two-photon fluorescence microscopy

Two-photon microscopy was performed as described[29], at λ = 750 nm, using a 60× water immersion objective. The temperature of GUVs on the microscope stage was controlled by means of a small water bath attached to the objective of an inverted microscope. The microscope objective was additionally kept at constant temperature and thermally isolated from the microscope stage. The temperature variation of our set-up is less than ±100 mK.

Vesicle compositions

Lipid compositions are expressed as mole fractions of sphingomyelin, DOPC and cholesterol, respectively. Vesicles shown in Fig. 1: 1a, 0.25/0.5/0.25; 1b, 0.585/0.1/0.315; 1c–f, 0.45/0.45/0.1; 1g and h, 0.615/0.135/0.25. Vesicles shown in Fig. 2: 2a, 0.56/0.24/0.2; 2b, 0.615/0.135/0.25; 2c and d, 0.675/0.075/0.25; 2e, 0.638/0.112/0.25; 2f, 0.675/0.075/0.25; 2g, 0.63/0.07/0.3; 2h, 0.585/0.102/0.313.

1. Käs, J. & Sackmann, E. Shape transitions and shape stability of giant phospholipid vesicles in pure water induced by area-to-volume changes. *Biophys. J.* **60,** 825–844 (1991).
2. Döbereiner, H. G., Käs, J., Noppl, D., Sprenger, I. & Sackmann, E. Budding and fission of vesicles. *Biophys. J.* **65,** 1396–1403 (1993).
3. Dietrich, C. *et al.* Lipid rafts reconstituted in model membranes. *Biophys. J.* **80,** 1417–1428 (2001).
4. Veatch, S. L. & Keller, S. L. Organization in lipid membranes containing cholesterol. *Phys. Rev. Lett.* **89,** 268101 (2002).
5. Lipowsky, R. Budding of membranes induced by intramembrane domains. *J. Phys. II France* **2,** 1825–1840 (1992).
6. Leibler, S. & Andelman, D. Ordered and curved meso-structures in membranes and amphiphilic films. *J. Phys.* **48,** 2013–2018 (1987).
7. Seul, M. & Andelman, D. Domain shapes and patterns: The phenomenology of modulated phases. *Science* **267,** 476–483 (1995).
8. Jülicher, F. & Lipowsky, R. Shape transformations of vesicles with intramembrane domains. *Phys. Rev. E* **53,** 2670–2683 (1996).
9. Andelman, D., Kawakatsu, T. & Kawasaki, K. Equilibrium shape of two-component unilamellar membranes and vesicles. *Europhys. Lett.* **19,** 57–62 (1992).
10. Jiang, Y., Lookman, T. & Saxena, A. Phase separation and shape deformation of two-phase membranes. *Phys. Rev. E* **61,** R57–R60 (2000).
11. Kumar, P. B. S., Gompper, G. & Lipowsky, R. Budding dynamics of multicomponent membranes. *Phys. Rev. Lett.* **86,** 3911–3914 (2001).
12. Helfrich, W. Elastic properties of lipid bilayers: Theory and possible experiments. *Z. Naturforsch.* **28c,** 693–703 (1973).
13. Jenkins, J. T. Static equilibrium configurations of a model red blood cell. *J. Math. Biol.* **4,** 149–169 (1976).
14. Seifert, U. Curvature-induced lateral phase separation in two-component vesicles. *Phys. Rev. Lett.* **70,** 1335–1338 (1993).
15. Duwe, H. P. & Sackmann, E. Bending elasticity and thermal excitations of lipid bilayer vesicles: Modulation by solutes. *Physica A* **163,** 410–428 (1990).
16. Benvegnu, D. J. & McConnell, H. M. Line tension between liquid domains in lipid monolayers. *J. Phys. Chem.* **96,** 6820–6824 (1992).
17. Schneider, M. B., Jenkins, J. T. & Webb, W. W. Thermal fluctuations of large quasi-spherical bimolecular phospholipid vesicles. *J. Phys.* **45,** 1457–1472 (1984).
18. Helfrich, W. & Servuss, R. M. Undulations, steric interactions and cohesion of fluid membranes. *Nuovo Cimento D* **3,** 137–151 (1984).
19. Chen, C.-M., Higgs, P. G. & MacKintosh, F. C. Theory of fission for two-component lipid vesicles. *Phys. Rev. Lett.* **79,** 1579–1582 (1997).
20. Lipowsky, R. & Dimova, R. Domains in membranes and vesicles. *J. Phys. Condens. Matter* **15,** S31–S45 (2003).
21. Samsonov, A. V., Mihalyov, I. & Cohen, F. S. Characterization of cholesterol-sphingomyelin domains and their dynamics in bilayer membranes. *Biophys. J.* **81,** 1486–1500 (2001).
22. Debregeas, G., de Gennes, P.-G. & Brochard-Wyart, F. The life and death of "bare" viscous bubbles. *Science* **279,** 1704–1707 (1998).
23. Andelman, D., Brochard, F. & Joanny, J. F. Phase transitions in Langmuir monolayers of polar molecules. *J. Chem. Phys.* **86,** 3673–3681 (1987).
24. Bar-Ziv, R. & Moses, E. Instability and "pearling" states produced in tubular membranes by competition of curvature and tension. *Phys. Rev. Lett.* **73,** 1392–1395 (1994).
25. Wintz, W., Döbereiner, H. G. & Seifert, U. Starfish vesicles. *Europhys. Lett.* **33,** 403–408 (1996).
26. Mukherjee, S. & Maxfield, F. R. Role of membrane organization and membrane domains in endocytic lipid trafficking. *Traffic* **1,** 203–211 (2000).
27. Huttner, W. B. & Zimmerberg, J. Implications of lipid microdomains for membrane curvature, budding and fission. *Curr. Opin. Cell Biol.* **13,** 478–484 (2001).
28. Mathivet, L., Cribier, S. & Devaux, P. F. Shape change and physical properties of giant phospholipid vesicles prepared in the presence of an AC electric field. *Biophys. J.* **70,** 1112–1121 (1996).
29. Denk, W., Strickler, J. H. & Webb, W. W. Two-photon laser scanning fluorescence microscopy. *Science* **248,** 73–76 (1990).

Cool Indonesian throughflow as a consequence of restricted surface layer flow

Arnold L. Gordon, R. Dwi Susanto & Kevin Vranes

Lamont-Doherty Earth Observatory, Columbia University, Palisades, New York 10964, USA

Approximately 10 million $m^3 s^{-1}$ of water flow from the Pacific Ocean into the Indian Ocean through the Indonesian seas[1]. Within the Makassar Strait, the primary pathway of the flow[2], the Indonesian throughflow is far cooler than estimated earlier, as pointed out recently on the basis of ocean current and temperature measurements[3,4]. Here we analyse ocean current and stratification data along with satellite-derived wind measurements, and find that during the boreal winter monsoon, the wind

drives buoyant, low-salinity Java Sea surface water into the southern Makassar Strait, creating a northward pressure gradient in the surface layer of the strait. This surface layer 'freshwater plug' inhibits the warm surface water from the Pacific Ocean from flowing southward into the Indian Ocean, leading to a cooler Indian Ocean sea surface[5–7], which in turn may weaken the Asian monsoon[8]. The summer wind reversal eliminates the obstructing pressure gradient, by transferring more-saline Banda Sea surface water into the southern Makassar Strait. The coupling of the southeast Asian freshwater budget to the Pacific and Indian Ocean surface temperatures by the proposed mechanism may represent an important negative feedback within the climate system.

The Indonesian throughflow (ITF) modifies the heat and freshwater budgets and air–sea heat fluxes of the Pacific and Indian oceans, and may exercise a role in the El Niño/Southern Oscillation (ENSO) and Asian monsoon climate phenomenon[5–9]. Observations show that the water composing the ITF is derived from the North Pacific thermocline[2,10], though at greater depth (water cooler than $6\,^{\circ}\mathrm{C}$) it is directly drawn from the South Pacific[2,10,11] (Fig. 1). In the past, the ITF temperature has been thought to be warm, $22\,^{\circ}\mathrm{C}$ (ref. 12) to $24\,^{\circ}\mathrm{C}$ (refs 13, 14). Recent measurements of the ITF within the Makassar Strait suggest that the transport-weighted

temperature is at least $9\,^{\circ}\mathrm{C}$ colder than earlier estimates[4].

The Indian-to-Pacific flow south of Tasmania, which balances the ITF, is cool, perhaps 6 to $8\,^{\circ}\mathrm{C}$ (ref. 7). If this water were to flow directly into the Indonesian seas without atmospheric contact, the ITF is expected to be similarly cool. However, water destined for the ITF criss-crosses the tropical Pacific within the upwelling regimes of the zonal equatorial currents, to enter the North Pacific subtropics before ultimate export to the Indian Ocean as the ITF[2], offering ample opportunity for substantial warming by the atmosphere. For example, warming of a 10-Sv ($1\,\mathrm{Sv} = 10^{6}\,\mathrm{m}^{3}\,\mathrm{s}^{-1}$) stream from $7\,^{\circ}\mathrm{C}$ to a typical upper thermocline temperature of $23\,^{\circ}\mathrm{C}$ over a period of 10 to 100 yr (a reasonable range of Pacific Ocean residence times for ITF-destined water) requires mere fractions of a $\mathrm{W\,m}^{-2}$, which is insignificant relative to the low-latitude heat exchange between the ocean and atmosphere of tens of $\mathrm{W\,m}^{-2}$. Thus it is likely that the cool stream from south of Tasmania would be substantially heated en route to the Indonesian seas. Inverse solutions[15–17] assume a steady-state ocean while using oceanographic sections obtained at different seasons or years, and may not be able to detect the subtleties of circulation pathways and heating of ITF waters within the Pacific Ocean. Although the ITF coolness may be a direct consequence of the large-scale circulation, as shown below it is more probably the result of a more localized mechanism within the
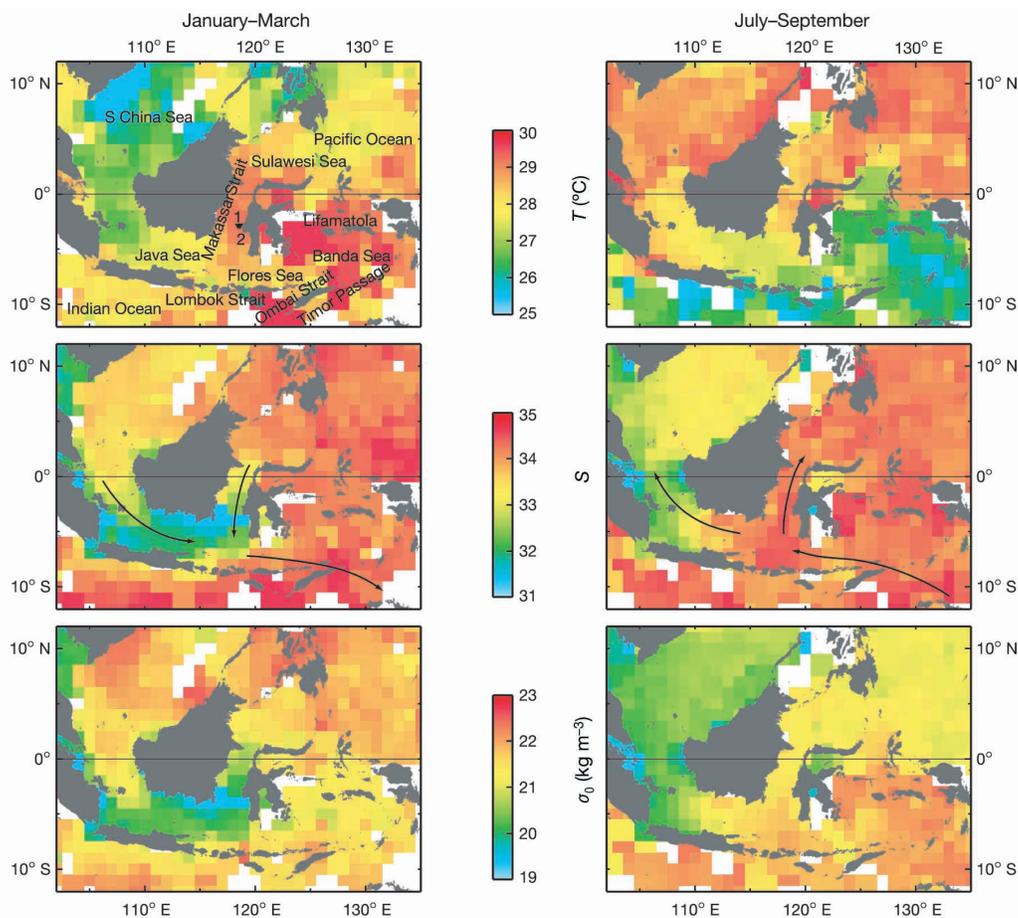
Figure 1 The Indonesian seas. Shown are the upper 20-m averages of summer and winter temperature (T), salinity (S) and density anomaly (σ_0) of the Indonesian seas (data from ref. 29). The prevailing monsoon winds are shown on the salinity panels; place names and the location of the two Makassar Strait moorings are shown on the January–March temperature panel. On 23 November 1996, the current meter mooring no. 1 was deployed at 2° 52′ S, 118° 27′ E in the 2,137 m deep, 45 km wide, Labani Channel of the Makassar Strait. Mooring no. 2 was deployed on 30 November just east of MAK-1 at 2° 51′ S, 118° 38′ E (ref. 18). The MAK moorings also included temperature sensors at 11 levels from 110 m and deeper[3]. During the northwest monsoon, January to March, the Java Sea low-salinity surface water shifts into the southern Makassar Strait. During the southeast monsoon, July to September, the southern Makassar Strait surface layer is more saline and less buoyant, as the southeast monsoon winds return the low-salinity water into the Java Sea. The buoyant surface water of the southern Makassar Strait inhibits southward transport within the surface layer during the northwest monsoon, despite southward wind within the Strait, lowering the temperature of the Indonesian throughflow.

Indonesian seas, which inhibits the transfer of warm Pacific surface water into the Indian Ocean.

Two moorings deployed in the Makassar Strait[18] (Fig. 1) carried upward-looking acoustic Doppler current profilers (ADCPs) set at 150 m, with four current meters at 200 m, 250 m, 350 m and 750 m. Though the moorings measured the ITF for 1.7 yr, owing to instrument failure the combined ADCP time series measured the surface layer flow for 7 months, from December 1996 through to June 1997. MAK-2 ADCP time series spans 3 months, ending in early March, and the MAK-1 ADCP (whose data were recently processed, overcoming a data recording problem) spans 7 months, ending in early July.

The Makassar Strait transport for 1997 was 9.3 Sv (ref. 18). This compares favourably with export to the Indian Ocean within the upper 680 m (sill depth of the Makassar Strait) of 7.3–10.7 Sv through the passages of the Sunda Islands: 5.6–9.0 Sv for the combined Timor Passage and Ombai Strait[19,20], and the Lombok Strait transport of 1.7 Sv (ref. 21). Although the measurements cited were made at different times, an ITF of 10 Sv or slightly larger seems reasonable.

The interocean heat transfer through the Indonesian seas depends on the relationship of the volume transport profile to the temperature profile. Estimates based on direct measurements of currents and temperature in the Makassar Strait from the MAK moorings argue for an ITF transport-weighted temperature of slightly less than 15 °C (ref. 4). It is unlikely that the Makassar Strait transport-weighted temperature can be increased from 15 °C to 24 °C before export to the Indian Ocean via the Sunda passages, as such heating requires an atmosphere-to-ocean heat flux of 580 W m^{-2}, an order of magnitude greater than the estimated air–sea heat flux of 50 W m^{-2} for this region[22].

The relatively cool ITF results from a restricted contribution of warm surface waters (Fig. 2). Within the ADCP record, the surface layer transport varies strongly with season, with low southward speeds interspersed with periods of northward flow during the northwest monsoon from December 1996 to March 1997. From April to the end of the ADCP record in early July 1997, the surface flow is primarily southward. Even when southward, the surface layer transport is never stronger than the thermocline (100–200 m) transport. From April to June 1997, during strong southward surface layer flow, the average transport within each of the two 50-m slabs between 100 and 200 m is 1.23 Sv, compared to 1.09 Sv in the upper 50 m.

We propose that a major factor in restricting a surface layer contribution to the ITF is the meridional buoyancy gradient set up within the Makassar Strait that accompanies the redistribution of low salinity Java Sea water (Fig. 1; Fig. 3). The low surface salinities of the Java and South China seas are due to heavy precipitation and large river runoff from Southeast Asia. During the northwest monsoon, the eastward zonal wind expels the low salinity, buoyant water of the shallow Java Sea into the surface layer of the southern Makassar Strait. During the remainder of the year, the winds are either weak (monsoon transition months) or directed westward (southeast monsoon), drawing more-saline surface waters of the Flores and Banda seas into the Java Sea, shifting buoyancy from the southern Makassar Strait into the western Java Sea and South China Sea. The seasonal change of surface layer buoyancy within the Sulawesi Sea at the northern end of the Makassar Strait is much
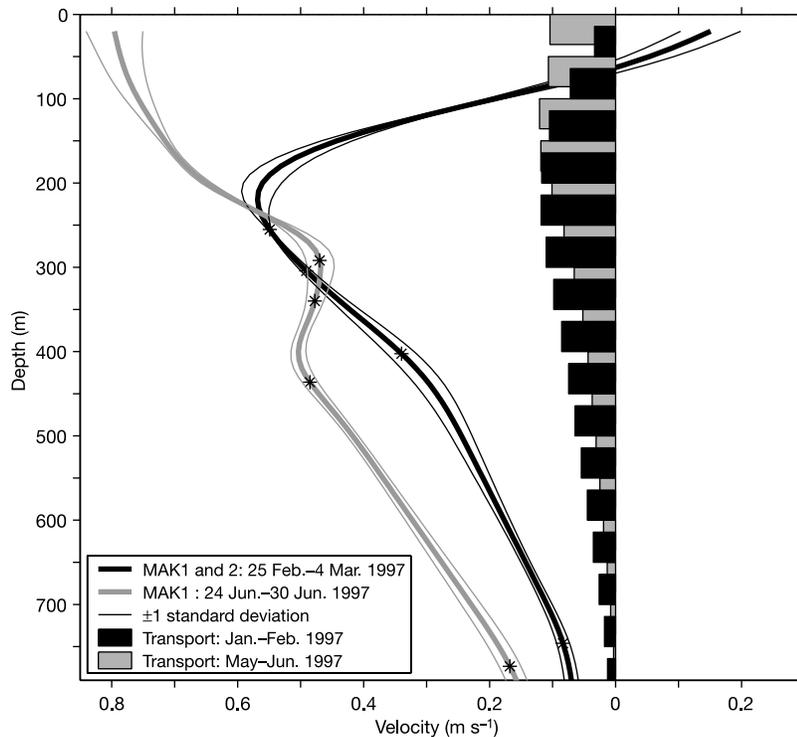
Figure 2 Profile of meridional velocity and transport as measured from mooring no. 1 (Fig. 1). The velocity profile (southward shown negative) with one standard deviation is shown for two periods: from 25 February to 4 March 1997 (the northwest monsoon, thick black line) and from 24 to 30 June 1997 (early southeast monsoon, thick grey line). The asterisks show the observed mean current and depth recorded at the four current meters for each of the two time periods. Above 150 m the curves are defined by the ADCP data. The southward transport in Sv (1 Sv = 10^6 m^3 s^{-1}) for 50 m depth bins is shown as a bar graph for January and February 1997 (black bars) representing the northwest monsoon, and for May and June 1997 (grey bars) representing the early southeast monsoon. The reduced surface layer southward flow during the northwest monsoon is evident in both the velocity and transport profiles. The velocity profiles are not shown for depths less than 20 m, as the surface data bins are contaminated by sea surface scatter of the acoustical energy. For the top 50 m bin, transport is calculated by linear extrapolation to the surface.

more subdued (Fig. 3), as it is connected to the less seasonally variable surface salinity of the western Pacific. The more-buoyant surface water during the northwest monsoon generates a northward pressure gradient (relative to 100 decibars) within the Makassar Strait (Fig. 3), inhibiting southward flow within the surface layer. Warm Sulawesi Sea surface water that is inhibited from flowing southward within Makassar Strait during the northwest monsoon does not instead pass southward east of Sulawesi island, as the surface current charts for that region is northward flow in that season[23,24]. Left unopposed, the meridional pressure gradient of the northwest monsoon would force surface water northward; however, the pressure gradient is opposed by the southward-directed wind (Fig. 1). The northward pressure gradient is removed during the southeast (summer) monsoon (Fig. 3). During the southeast monsoon the buoyancy-induced meridional pressure gradient is close to zero, but then the Makassar wind is directed towards the north (Fig. 1).

The observed Makassar Strait surface layer flow correlates with regional winds measured by the NSCAT satellite. The average 'relative' meridional current for the upper 50 m (Fig. 4) is directed towards the north from early December until late March, tracking the Java Sea zonal wind with a correlation of 0.8. The Java zonal wind becomes persistently eastward in early December 1996, and remains eastward until mid-March 1997. The Java wind leads the meridional surface currents by about ten days, probably the time it takes for a wind reversal in Java Sea to shift the low surface salinity water. Although the Java wind is clearly a dominant factor, the wind within the Makassar Strait does play a role in higher frequency variability of the surface flow. The Makassar surface layer flow displays a few strong northward events, notably in late December (event A in Fig. 4) and in mid-January (C in Fig. 4). In the first few

days of January there is a brief episode of strong southward flow (B in Fig. 4). The northward current events correlate at 3-day lag with weaknesses or reversals in the prevailing southward-directed winds. Similarly, the southward current period correlates with a strong southward wind event. The surface layer meridional current is weakly southward at the end of March, following the reversal of the Java Sea zonal winds by a week. The southward surface layer flow becomes predominant in mid-June as the westward Java Sea wind becomes more persistent.

The seasonal shift of low-salinity Java Sea water into the southern Makassar Strait acts as a 'freshwater plug' during the northwest monsoon, which effectively inhibits the Makassar Strait surface water from freely flowing southward. The cool ITF is a direct result of suppressed surface layer flow, as deeper, colder layers then dominate the full-column transport. During the southeast monsoon the 'freshwater plug' is removed, allowing southward transport in the surface layer, though northward wind is expected to hinder this effect.

Changes in the freshwater budget of the western Indonesian seas and Southeast Asian monsoon winds would be expected to alter the intensity of the 'freshwater plug'. Greater amounts of freshwater expelled from the Java Sea into the southern Indonesian seas would induce a colder ITF (lesser amounts would lead to a warmer ITF). As the regional precipitation changes with the phase of ENSO, Asian monsoon and at longer temporal scales, the ITF temperature may adjust accordingly. A strong 'freshwater plug' would reduce transfer of the western Pacific's warm pool into the Indian Ocean, with potential feedback to ENSO. The Indian Ocean surface layer would receive less Pacific heat, affecting its surface temperature and altering the pattern of heat and water vapour exchange with the atmosphere, presumably influencing the
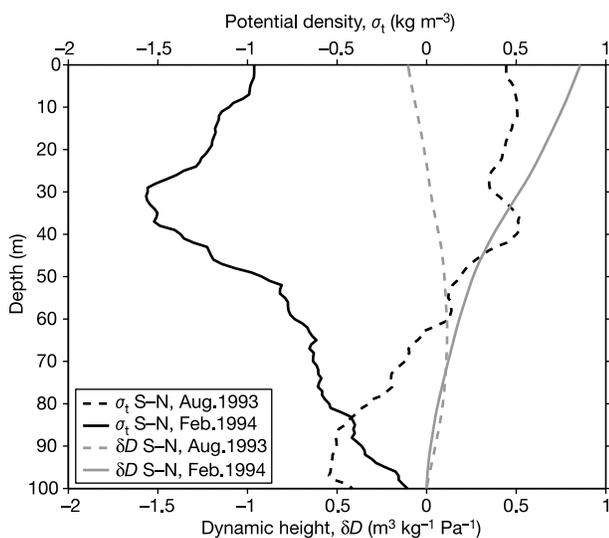
Figure 3 Differences in density and dynamic height within the upper 100 m between the northern and southern Makassar Strait (northern subtracted from southern) for two monsoon phases. In February 1994, (solid black line) representing the northwest monsoon, the density difference from the sea surface to a depth of 100 m is negative, meaning that the southern density profile is less dense or more buoyant than the northern profile. During August 1993 (solid grey line), representing the southeast monsoon, the density difference along the Makassar Strait is relatively small but positive in the upper 60 m. The dynamic height anomalies of the isobaric surfaces from 0 to 100 decibars (1 db is approximately equivalent to 1 m) relative to 100 db are shown as dashed lines. During the northwest monsoon (dashed black line), the surface layer isobaric surfaces in the southern Makassar Strait are higher than they are in the north, signifying a northward pressure gradient within the surface layer. During the southeast monsoon (dashed grey line), the meridional pressure gradient within the surface layer is essentially zero.
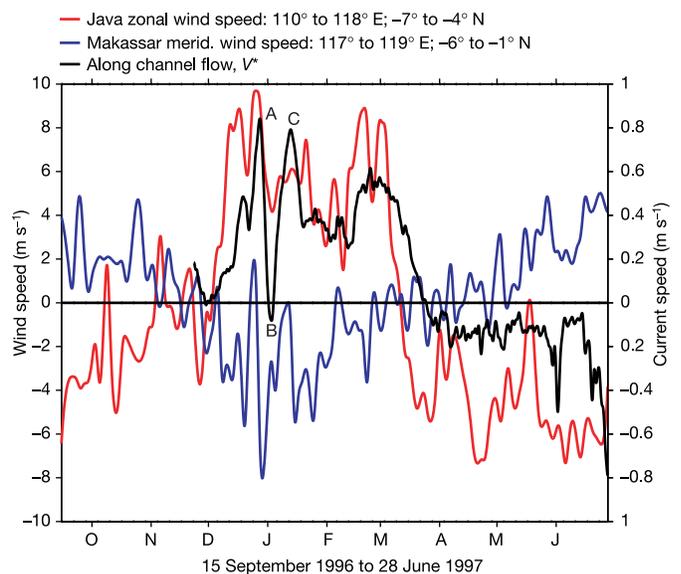
Figure 4 Makassar Strait surface layer current and Java and Makassar wind time series. The along-channel 'relative' surface layer current in the Makassar Strait (V^*, solid black line) is shown for the period of the ADCP time series. The values are daily averages; the 'relative' surface current curve is produced by subtracting the meridional current as measured within the thermocline by a current meter near 200 m from the average meridional current of the upper 50 m of the water column as measured by the ADCP. This removes the larger-scale ITF component from the more locally forced surface layer flow. The zonal wind in Java Sea (red line) and the meridional wind in Makassar Strait (blue line) reveal the close relationship of the wind of these two areas to the surface current. The wind data are derived from two-day-averaged wind as measured by the NSCAT satellite. The letters A, B and C denote the three events discussed in the text.

letters to nature

Asian monsoon and the Indian Ocean dipole[25,26].

Models have been used to investigate the regional effect of varying the magnitude of the ITF on the Indian Ocean upper layer heat content and sea surface temperature[5–9]. Changes in the sea surface temperature associated with changes in the ITF transport shift the position of the deep atmosphere convection region of the western tropical Pacific[8,27] and, by changing the sea surface temperature in the Indian Ocean, alter the net evaporation within the Indian Ocean with consequences for the monsoon[7,8,28]. Although models investigate the contrast between 'off' and 'on' ITF[5–9], they do not explicitly consider the effects or causes of varying the ITF transport and temperature profiles, yet changes in their relationship, even without changes in the net transport, may be expected to alter the sea surface temperature and heat budget of the Pacific and Indian oceans and associated climate phenomena. □

1. Gordon, A. L. in *Ocean Circulation and Climate: Observing and Modeling the Global Ocean* (ed. Gould, J.) 303–314 (Academic, San Diego, 2001).
2. Gordon, A. L. & Fine, R. A. Pathways of water between the Pacific and Indian Oceans in the Indonesian seas. *Nature* **379,** 146–149 (1996).
3. Ffield, A., Vranes, K., Gordon, A. L., Susanto, R. D. & Garzoli, S. L. Temperature variability within Makassar Strait. *Geophys. Res. Lett.* **27,** 237–240 (2000).
4. Vranes, K., Gordon, A. L. & Ffield, A. The heat transport of the Indonesian Throughflow and implications for the Indian Ocean heat budget. *Deep-Sea Res. II* **49,** 1391–1410 (2002).
5. Lee, T., Fukumori, I., Menemenlis, D., Xing, Z. & Fu, L. Effects of the Indonesian Throughflow on the Pacific and Indian Oceans. *J. Phys. Oceanogr.* **32,** 1404–1429 (2002).
6. Hirst, A. C. & Godfrey, J. S. The role of Indonesian Throughflow in a global ocean GCM. *J. Phys. Oceanogr.* **23,** 1057–1086 (1993).
7. Godfrey, S. The effect of the Indonesian Throughflow on ocean circulation and heat exchange with the atmosphere: A review. *J. Geophys. Res.* **101,** 12217–12237 (1996).
8. Wajsowicz, R. Air-sea interaction over the Indian Ocean due to variations in the Indonesian Throughflow. *Clim. Dyn.* **18,** 437–453 (2002).
9. Wajsowicz, R. & Schneider, E. K. The Indonesian throughflow's effect on global climate determined from the COLA coupled climate system. *J. Clim.* **14,** 3029–3042 (2001).
10. Ilahude, A. G. & Gordon, A. L. Thermocline stratification within the Indonesian Seas. *J. Geophys. Res.* **101,** 12401–12409 (1996).
11. Van Aken, H. M., Punjanan, J. & Saimima, S. Physical aspects of the flushing of the east Indonesian basins. *Neth. J. Sea Res.* **22,** 315–339 (1988).
12. Piola, A. R. & Gordon, A. L. On oceanic heat and fresh-water fluxes at 30°S. *J. Phys. Oceanogr.* **16,** 2184–2190 (1986).
13. Toole, J. M. & Warren, B. A. A hydrographic section across the subtropical South Indian Ocean. *Deep-Sea Res. I* **40,** 1973–2019 (1993).
14. Robbins, P. E. & Toole, J. M. The dissolved silica budget as a constraint on the meridional overturning circulation of the Indian Ocean. *Deep-Sea Res. I* **44,** 879–906 (1997).
15. Macdonald, A. M. Property fluxes at 30S and their implications for the Pacific-Indian throughflow and the global heat budget. *J. Geophys. Res.* **98,** 6851–6868 (1993).
16. Ganachaud, A. & Wunsch, C. Improved estimates of global ocean circulation, heat transport and mixing from hydrographic data. *Nature* **408,** 453–457 (2000).
17. Ganachaud, A. & Wunsch, C. Large-scale ocean heat and freshwater transports during the World Ocean Circulation Experiment. *J. Clim.* **16,** 696–705 (2003).
18. Gordon, A. L., Susanto, R. D. & Ffield, A. Throughflow within Makassar Strait. *Geophys. Res. Lett.* **26,** 3325–3328 (1999).
19. Molcard, R., Fieux, M. & Ilahude, A. G. The Indo-Pacific throughflow in the Timor Passage. *J. Geophys. Res.* **101,** 12411–12420 (1996).
20. Molcard, R., Fieux, M. & Syamsudin, F. The throughflow within Ombai Strait. *Deep-Sea Res. I* **48,** 1237–1253 (2001).
21. Murray, S. P. & Arief, D. Throughflow into the Indian Ocean through the Lombok Strait, January 1985–January 1986. *Nature* **333,** 444–447 (1988).
22. Oberhuber, J. M. *An Atlas Based on "COADS" Data Set* (Tech. Rep. 15, Max-Planck-Institut für Meteorologie, Hamburg, 1988).
23. Wyrtki, K. *Physical Oceanography of the Southeast Asian Waters* (NAGA Rep. 2, Scripps Institution of Oceanography, La Jolla, 1961).
24. Mariano, A. J., Ryan, E. H., Perkins, B. D. & Smithers, S. *The Mariano Global Surface Velocity Analysis* 55 (United States Coast Guard, Washington DC, 1995).
25. Saji, N. H., Goswami, B. N., Vinayachandran, P. N. & Yamagata, T. A dipole mode on the tropical Indian Ocean. *Nature* **401,** 360–363 (1999).
26. Susanto, R. D., Gordon, A. L. & Zheng, Q. N. Upwelling along the coasts of Java and Sumatra and its relation to ENSO. *Geophys. Res. Lett.* **28,** 1599–1602 (2001).
27. Schneider, N. The Indonesian throughflow and the global climate system. *J. Clim.* **11,** 676–689 (1998).
28. Wajsowicz, R. C. & Schopf, P. S. Oceanic influences on the seasonal cycle in evaporation over the Indian Ocean. *J. Clim.* **14,** 1199–1226 (2001).
29. Conkright, M. E. *et al. World Ocean Atlas CD-ROM Data Set Documentation* (Internal Report 15, National Oceanographic Data Center, Silver Spring, Maryland, 1998).

Correspondence and requests for material should be addressed to A.L.G. (agordon@ldeo.columbia.edu).

....

Independent rate and temporal coding in hippocampal pyramidal cells

John Huxter[1]*, **Neil Burgess**[1,2] & **John O'Keefe**[1,2]

[1]*Department of Anatomy and Developmental Biology,* [2]*Institute of Cognitive Neuroscience, University College London, Gower Street, London, UK*

* Present address: Department of Anatomy, University of Bristol

....

In the brain, hippocampal pyramidal cells use temporal[1] as well as rate[2] coding to signal spatial aspects of the animal's environment or behaviour. The temporal code takes the form of a phase relationship to the concurrent cycle of the hippocampal electroencephalogram theta rhythm[1]. These two codes could each represent a different variable[3,4]. However, this requires the rate and phase to vary independently, in contrast to recent suggestions[5,6] that they are tightly coupled, both reflecting the amplitude of the cell's input. Here we show that the time of firing and firing rate are dissociable, and can represent two independent variables: respectively the animal's location within the place field, and its speed of movement through the field. Independent encoding of location together with actions and stimuli occurring there may help to explain the dual roles of the hippocampus in spatial and episodic memory[7,8], or may indicate a more general role of the hippocampus in relational/declarative memory[9,10].

A cell must fire to manifest either a temporal or a rate code. Place cells are hippocampal pyramidal cells that increase their firing rate in a particular portion of the environment[2,11] (the 'place field', Fig. 1b). As such, they provide a coarse rate code for the animal's location within which a temporal code provides additional information[1,12,13]. In addition, we propose that the rate of firing within the field can vary to encode for other information without disrupting this temporal code.

We recorded the firing of place cells and the electroencephalogram (EEG) from the hippocampi of rats as they ran back and forth on a linear track for food reward at each end (Fig. 1a, Methods). During this behaviour, the EEG shows the prominent theta oscillation and each place cell fires in a specific region of the track (Fig. 1b). The cell's bursting rate through the field (Fig. 1c) is slightly higher than the concurrent EEG theta frequency, so that the average phase of firing moves earlier on each theta wave as the animal progresses through the field (Fig. 1d). The phase of firing correlates with spatial variables such as the animal's position on the track or within the field (Fig. 1d), and also with non-spatial variables such as the time since entry into the field (Fig. 1e) or instantaneous firing rate (IFR; Fig. 1f), but in general the correlation with position is stronger than with either (Fig. 1g; see also refs 1, 5, 6, 12). Some process must align the phase of each spike relative to the concurrent theta wave so that the phase codes for location despite the different speeds of each run through the field.

Must the phase and rate codes always co-vary with each other, or